Hindawi
Journal of Advanced Transportation
Volume 2017, Article ID 6510747, 14 pages
https://doi.org/10.1155/2017/6510747

WILEY | Hindawi

Research Article

State-of-Charge Estimation and Active Cell Pack Balancing Design of Lithium Battery Power System for Smart Electric Vehicle

Z. C. Gao,[1] C. S. Chin,[2] W. D. Toh,[1] J. Chiew,[1] and J. Jia[1]

[1] *Clean Energy Research Centre, School of Engineering, Temasek Polytechnic, 21 Tampines Avenue 1, Singapore 529757*
[2] *Faculty of Science, Agriculture, and Engineering, Newcastle University in Singapore, Singapore*

Correspondence should be addressed to C. S. Chin; cheng.chin@ncl.ac.uk

Received 7 July 2017; Revised 26 October 2017; Accepted 13 November 2017; Published 31 December 2017

Academic Editor: Emanuele Crisostomi

Copyright © 2017 Z. C. Gao et al. This is an open access article distributed under the Creative Commons Attribution License, which permits unrestricted use, distribution, and reproduction in any medium, provided the original work is properly cited.

This paper presents an integrated state-of-charge (SOC) estimation model and active cell balancing of a 12-cell lithium iron phosphate (LiFePO4) battery power system. The strong tracking cubature extended Kalman filter (STCEKF) gave an accurate SOC prediction compared to other Kalman-based filter algorithms. The proposed groupwise balancing of the multiple SOC exhibited a higher balancing speed and lower balancing loss than other cell balancing designs. The experimental results demonstrated the robustness and performance of the battery when subjected to current load profile of an electric vehicle under varying ambient temperature.

1. Introduction

Lithium-ion battery storage system plays a vital role in electric vehicle (EV) applications [1–5]. Portable lithium batteries are commonly used for their high energy density and low cost. However, the voltages of these battery cells are quite low and require many battery cells in series to meet the voltage requirement for real applications. In addition, there exist many problems with the battery management system (BMS) such as inaccurate state-of-charge (SOC) estimation due to multiple charging and discharge of the cells. Hence, the SOC [6] was one of the essential parameters to estimate in order to prevent damage to the battery. Unfortunately, the estimation of SOC is not a simple process as it depends on factors such as battery's capacitance, resistance, internal temperature, ambient temperature [7, 8], and other cell characteristics. The ratio of the charge delivered to the battery over the total charge of the battery was typically used to obtain the SOC.

The common ampere-hour integral method caused biases due to the integration. On the other hand, the voltage method used the battery voltage and SOC relationship or discharge curve to determine the SOC. The battery cell needs to disconnect from the load in order to determine the open-circuit voltage during actual battery operation. Another approach based on equivalent circuit model (ECM) [9–12] was used to estimate the SOC. The resistors and capacitors were used for modeling the battery cell in ECM. Although it requires an experiment to validate the parameters, it is relatively easy to use and implement. However, the battery is a nonlinear time-varying system with capacity changes due to aging, and ambient temperature variation, an accurate estimation of the SOC on the ECM, is therefore required.

Another approach using fuzzy logic [13] was proposed to estimate the SOC of the lithium-ion battery in EV. It utilized both battery terminal voltages to overcome the problem of overdischarging. The rules of combining membership functions were not robust due to the types of the battery cell used. The active cell balancing for multicell battery was not discussed.

As a result, a nonmodel based approach such as neural network [14–16] and its combination with fuzzy logic named fuzzy-neural network [17] was used. The support vector machine [18] was also used to estimate the battery dynamics. Although the neural network based approach and SVM were both a nonlinear estimation method that does not require the battery model [19, 20], a significant dataset and

computational time for training the SOC value were required. To circumvent the issue of training time, the extreme machine learning (ELM) [21–25] was proposed that uses regularized least squares to compute faster than the conventional quadratic programming approach without tuning the hidden to output neurons. Nevertheless, a significant dataset for an accurate SOC estimation was required despite the short training time. Moreover, the application of a multicell SOC estimation and cell balancing was not proposed.

Instead of nonmodel based approach, a more accurate physical modeling using electrochemical model was used [26–29]. The electrochemical model provided an accurate physical meaning of the electrical and chemical properties of the battery cell. The nonlinear partial differential equations increased the model complexity and computational time during SOC estimation. As a result, a linear model using fewer parameters in the electrochemical model was adopted [30] with Kalman filter (KF) to estimate the SOC. The extended Kalman filter (KF) [31–33], sliding-mode observer [34, 35], and Luenberger observer [36, 37] were applied to estimate the SOC using the ECM model. However, it required an accurate model of the battery and higher computing resource with correct initialization of parameters that changed rapidly.

The extended KF (EKF) was then proposed to estimate the SOC using a nonlinear ordinary differential equation model [38]. The unscented KF was utilized [39] to avoid such linearization of the nonlinear equation in EKF. A nonlinear SOC estimator [40] was then employed on the electrochemical model of the battery instead of the ECM. But the computation time and numerical error increased due to the numerical approach used in solving the partial differential equations. In addition, it could not track the sudden change in the SOC value. A strong tracking cubature Kalman filter (CKF) [41] that outperformed the EKF was proposed to track the sudden change of SOC value accurately. It was followed by the multirate strong tracking extended Kalman filter (STEKF) [42] to handle a higher dimensional state estimation of SOC. However, the paper demonstrated on a six-cell battery stack without using the CKF to track the fast-changing SOC value. Hence, the use of the strong tracking cubature on extended Kalman filter (STCEKF) with cell balancing is desired. Furthermore, most of the literature that involved SOC estimation was mainly dealt with theoretical development and comparisons with other SOC estimation methods on a single cell.

In addition to SOC estimation, an active cell balancing (AB) circuit [43–45] is another important element in the battery management system. Most batteries are made up of multiple cells that required AB to prevent each cell from overcharge or discharge after the SOC was determined. Although the topics of SOC estimation and active balancing were separately analyzed or published, it is essential to examine how a battery power system with both SOC estimation and AB can be realized.

With cell balancing, the battery cell lifetime and capacity can be further extended. In general, there exist two different AB circuits. The first type consumed the redundant energy of parallel resistance to maintain the terminal voltage of the cells. The second type used inductors, converters, or transformers to realize energy transfer between cells. The energy in the cells with higher SOC or terminal voltage can be transferred to other cells to maintain the same SOC and voltage among the cells. The disadvantage was the complexity of controlling the converters [41, 46–48]. A multistage equalization was used to simplify the circuit and increase the balancing speed.

There exist different cell balancing methods using a resistor, capacitor, inductor/transformer, and energy converter balancing method [44, 45]. For example, the shuttling capacitors cell balancing method named "charge shuttling cells equalization" used capacitors as external energy storage for alternating the energy between the cells for charge balancing. The control strategy was straightforward and efficient. But the disadvantages were the relatively long balancing time and high cost as compared to the passive balancing method. However, the shuttling capacitors can be optimized using a double-tiered switched capacitor (STSC) based on the switched capacitor to decrease the balancing time.

Another energy conversion cell balancing topology using inductors was used to move energy from a cell to another cell. The relative high balancing current provided a shorter balancing time. However, the inductor topology was relatively costly with high balancing losses. The energy converters such as Cuk, Buck-Boost, full-bridge PWM energy, and Quasi-Resonant Converter were used for cell balancing. When the imbalance was detected, the converters allowed the energy to transfer between cells. This method was used for high power applications. But they can be expensive and quite complex to control.

Hence, a proposed multicell battery power system with both SOC estimation and AB has the following contributions. The novelty will come from the proposed AB circuit to accomplish the groupwise balancing of the multiple SOC obtained via the STCEKF. The AB circuit consists of a switching circuit using a DC-DC converter, IGBT drivers, inductors, and diodes to balance the SOC among the cells. Each cell uses a single fast driver to reduce the balancing loss by controlling the cells' discharge, charge, and cut-off. The battery packs will be divided into groups to balance the energy simultaneously by transferring the energy from the cell with higher to lower SOC. In summary, a new integrated STCEKF model-based SOC estimation and the active cell balancing will be implemented on a multicell LiFePO4 battery power system to improve its performance and robustness in an electric vehicle.

The paper is organized as followed. In Section 2, a proposed battery design is presented followed by Section 3 of SOC estimation. In Section 4, describes the experimental results of the battery pack using actual load followed by the conclusion in Section 5.

2. Proposed Battery Power System Design

The nominal voltage and continuous discharge current of a single LiFePO4 cell (ANR26650M1-B) are limited to 3.3 V and 50 A, respectively. As shown in Figure 1, the battery pack consists of 12 cells connected in series to produce 2 kWh.

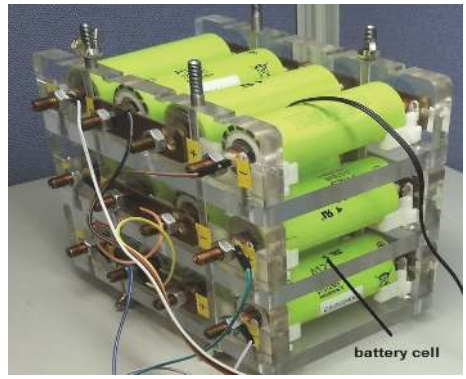

Figure 1: Proposed lithium iron phosphate battery prototype.

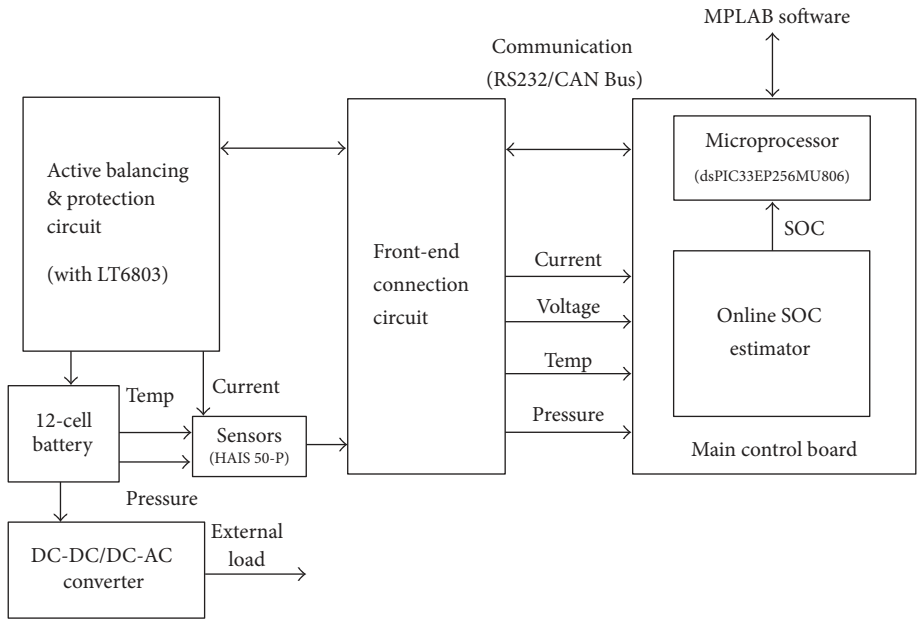

Figure 2: Proposed battery management system architecture with several subsystems for SOC estimation and active cell balancing.

An open frame design was used to accommodate all circuit boards, sensors, and battery cells in the prototyping stage.

The battery management system (BMS) will perform SOC estimation and active cell balancing on a single board. Figure 2 shows the proposed subsystems used in the architecture of the BMS board. Based on the power consumption, the main control board will compute the desired voltage and current. A lookup table will be used to record the optimal current and voltage of the battery at different power and voltage condition. A DC/DC converter will be used to interface between the cells and external load. The active balancing and protection (ABP) circuit will balance the SOC among the 12 cells via the multicell battery stack monitoring using the LT6803 chip. The analog signals from the current, voltage, temperature, and pressure sensor will be processed in the front-end connection (FEC) circuit. The measured data from the sensor will be transmitted via the serial port of the microprocessor. The control signal will send to the 12 cells via the ABP and FEC circuits. The online SOC estimator in Figure 2 can estimate the SOC based on the sampled data obtained via the front-end connection circuit. The SOC estimation and cell balancing algorithms were coded in C++ via MPLAB software on the host computer or laptop.

The active balancing circuit consists of relays, DC-DC converters, and current transducers. The relays and DC-DC converters were connected to the batteries as shown in Figure 3. The relays are represented by the switch symbols. One DC-DC converter (DC/DC2) was used to balance Cell #1 to Cell #6 (i.e., Pack #1) and another DC-DC converter (DC/DC1) was used to balance Cell #7 to Cell #12 (i.e., Pack #2). As shown in the inputs of the DC/DCs in Figure 3, the DC/DC2 was powered by Cell #8 to Cell #12 while DC/DC1 was powered by Cell #1 to Cell #5. Relays were employed to make these connections and enable the connections from DC/DC2 output to Cell #1 to Cell #6 and DC/DC1 output to Cell #7 to 12 independently. There exist four current

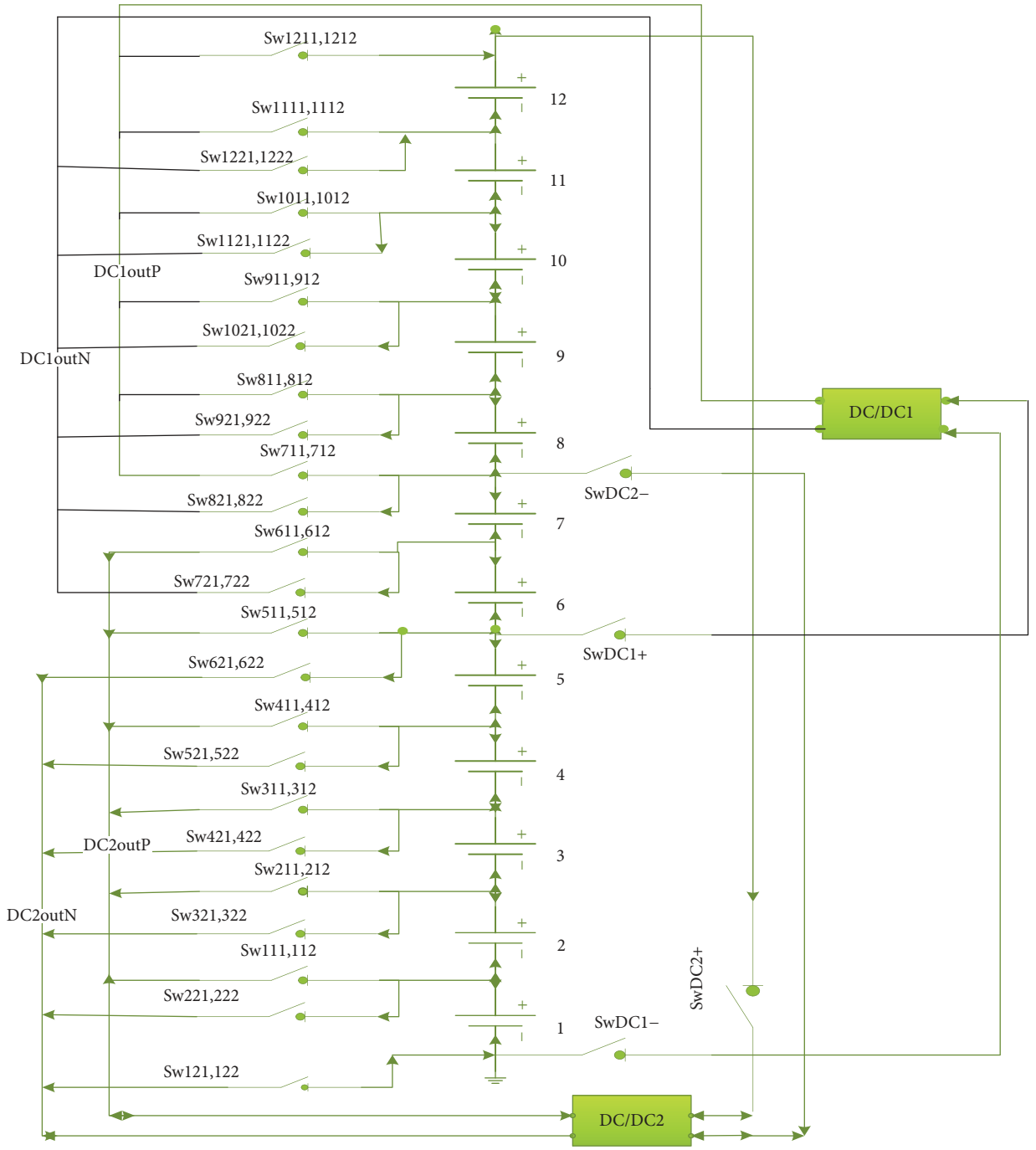

Figure 3: Active cell balancing scheme.

transducers to monitor the current drawn and delivered by both the DC-DC converters. The current transducers were configured to measure ±2 A, ±3 A, or ±6 A.

The flowchart of the active cell balancing is shown in Figure 4. Firstly, the system checks for any abnormalities condition using the estimated SOC. If the SOC is lower or higher than a preset limit, the cell will not be used. The remaining normal cells will be deployed. The SOC for each cell in a group of six will be ranked. There exist two groups of six cells, namely, Pack #1 and Pack #2. The cells with unequal voltages will be balanced. For example, the cell with highest SOC will be discharged while the cell with lowest SOC will be charged sequentially until the cells have equal voltage levels. The duration of the cycle depends on the time taken for the cells' balancing.

3. SOC Estimation

Many techniques were proposed for SOC estimation. However, the equivalent circuit model in Figure 5 was used. This

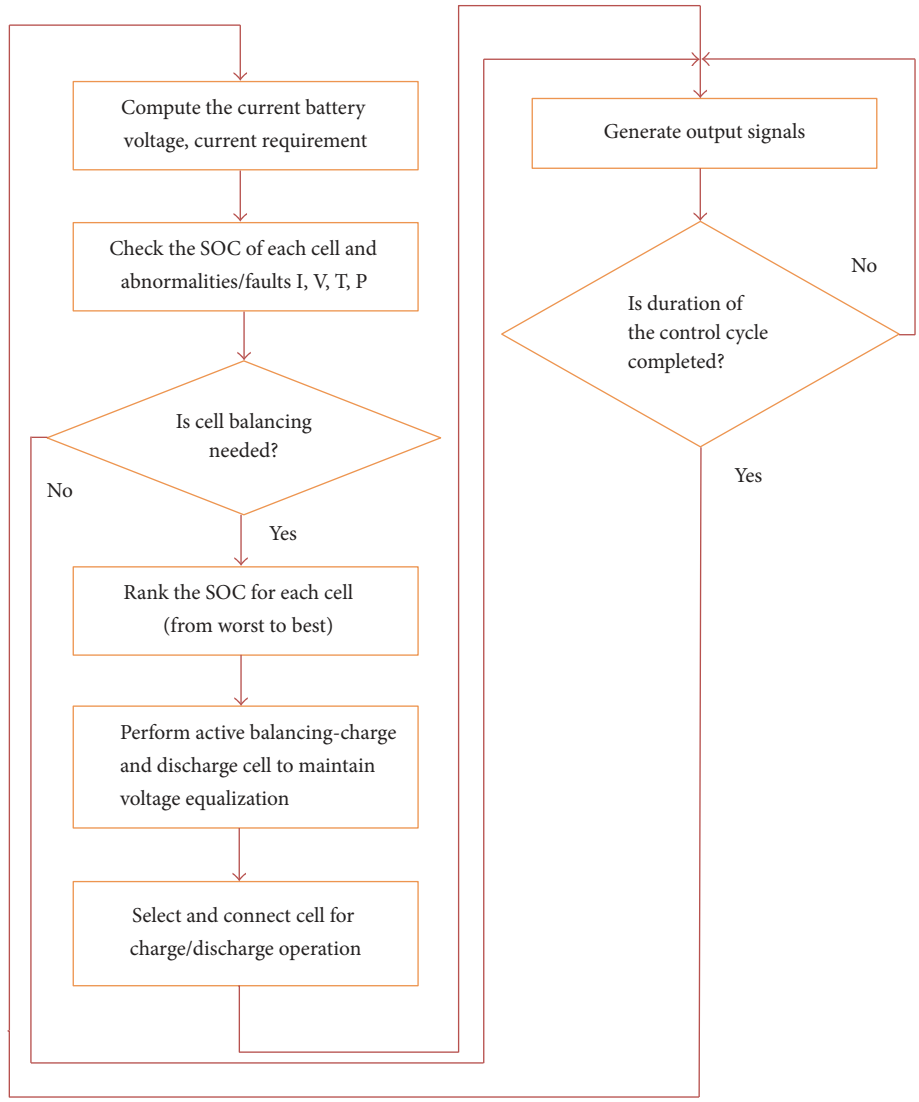

Figure 4: Active cell balancing algorithm flowchart.

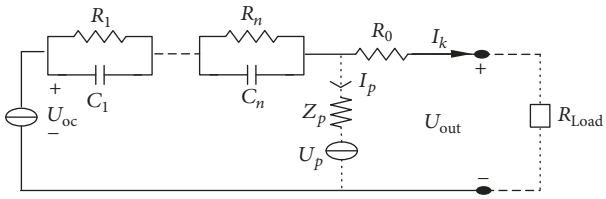

Figure 5: Classical topology of Thevenin equivalent circuit model.

model consists of open-circuit voltage (OCV) source U_{oc} with an indefinite number of parallel RC branches and a series resistance R_0. The model also contains a parasitic branch that represents self-charge and charging losses denoted by I_p. Instead of using indefinite RC branches as seen in Figure 5, a 2-RC equivalent circuit was used. The MATLAB/Simscape was utilized to model the cell's SOC using the 2-RC equivalent circuit. As seen in Figure 6, the Simscape model consists of five lookup tables, namely, $R0$, $R1$, $C1$, $R2$, and $C2$ at a different ambient temperature from 5°C to 45°C. The data in the lookup data was further optimized using the Parameter Estimation Toolbox at different SOC. The different 2-RC parameters at various SOC are tabulated in Table 1.

The dynamic equation of SOC can be given as

$$\dot{\text{SOC}} = -\frac{\eta I(t)}{C_n}, \tag{1}$$

where C_n is the battery cell capacity and η is the coulomb efficiency.

From the structure in Figure 5, the dynamic equations of the voltages U_1 and U_2 can be expressed as

$$\dot{U}_1 = \frac{I}{C_1} - \frac{U_1}{R_1 C_1},$$
$$\dot{U}_2 = \frac{I}{C_2} - \frac{U_2}{R_2 C_2}. \tag{2}$$

Table 1: Parameters of 2-*RC* equivalent circuit model.

SOC	R_0 (ohm)	R_1 (ohm)	R_2 (ohm)	C_1 (F)	C_2 (F)
0.05	0.0215	0.0152	0.0148	38848.99	90150.93
0.10	0.0026	0.0032	0.0020	1294.020	179973.3
0.19	0.0042	0.0046	0.0023	20618.27	636416.8
0.28	0.0033	0.0030	0.0024	10690.21	207895.2
0.37	0.0033	0.0018	0.0030	3880.350	117578.1
0.46	0.0026	0.0035	0.0013	67312.19	12303.82
0.54	0.0045	0.0001	0.0044	3643.250	111455.1
0.63	0.0056	0.0027	0.0006	318347.7	85798.68
0.72	0.0032	0.0036	0.0010	47656.71	11604.30
0.81	0.0022	0.0012	0.0019	1026.310	141113.7
0.90	0.0033	0.0027	0.0019	23379.15	432980.6
0.99	0.0101	0.0026	0.0027	12565.53	66708.01

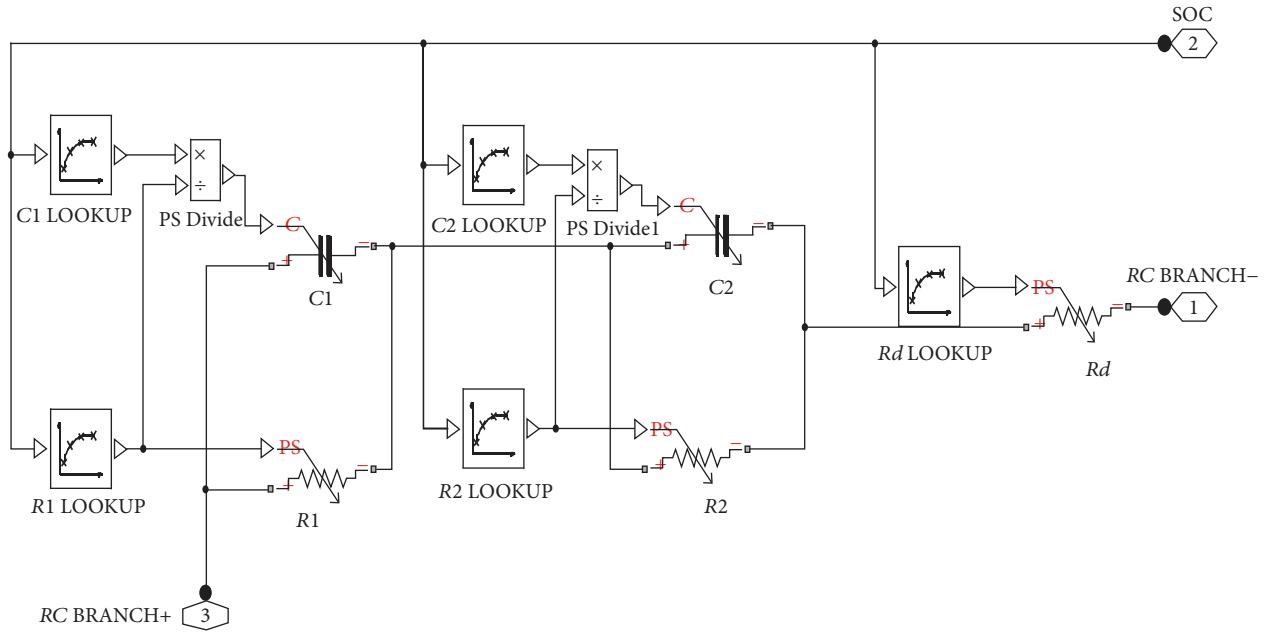

Figure 6: 2-*RC* equivalent circuit model of battery cell.

The battery terminal voltage can be written as

$$U_L = U_{oc} - IR_0 - U_1 - U_2, \tag{3}$$

where U_{oc} can be estimated by polynomial fitting. It is a standard method to determine the relationship between U_{oc} and SOC. But the errors are apparent during the end of the charging and discharging period. To compensate the fitting error, an exponential function and natural logarithm function are used

$$\begin{aligned} U_{oc}(\mathrm{SOC}) &= a_0 + a_1 \mathrm{SOC} + a_2 \log \mathrm{SOC} \\ &\quad + a_3 \log(1 - \mathrm{SOC}), \end{aligned} \tag{4}$$

where a_0, a_1, a_2, and a_3 are identified through open-circuit voltage- (OCV-) SOC curve fitting method.

The battery model has to be discretized in order to program the SOC algorithm into the microcontroller. In discrete time, the SOC dynamics can be given as follows:

$$\mathrm{SOC}(k) = \mathrm{SOC}(k-1) - \frac{\eta I(k) \Delta t}{C_n}, \tag{5}$$

where Δt is the sampling time interval.

The discrete time versions of (2) can be obtained by using zero-order hold (ZOH) process. The transformed equations are expressed as follows:

$$\begin{aligned} U_1(k+1) &= e^{-\Delta t/R_1C_1} U_1(k) + R_1\left(1 - e^{-\Delta t/R_1C_1}\right) I(k), \\ U_2(k+1) &= e^{-\Delta t/R_2C_2} U_2(k) + R_2\left(1 - e^{-\Delta t/R_2C_2}\right) I(k). \end{aligned} \tag{6}$$

Define the state vector $x_k = [\mathrm{SOC}(k)\ U_1(k)\ U_2(k)]^T$; the following state space model of the battery cell in discrete matrix form can be obtained:

$$\begin{bmatrix} \mathrm{SOC}(k) \\ U_1(k) \\ U_2(k) \end{bmatrix} = \begin{bmatrix} 1 & 0 & 0 \\ 0 & e^{-\Delta t/R_1C_1} & 0 \\ 0 & 0 & e^{-\Delta t/R_2C_2} \end{bmatrix} \begin{bmatrix} \mathrm{SOC}(k-1) \\ U_1(k-1) \\ U_2(k-1) \end{bmatrix} + \begin{bmatrix} -\dfrac{\eta I(k)\Delta t}{C_n} \\ R_1\left(1-e^{-\Delta t/R_1C_1}\right) \\ R_2\left(1-e^{-\Delta t/R_2C_2}\right) \end{bmatrix} I(k-1) + w(k-1). \tag{7}$$

The battery terminal voltage at any time sample k is written as such

$$U_L(k) = U_{\mathrm{oc}}(\mathrm{SOC}(k)) - I(k)R_0 - U_1(k) - U_2(k). \tag{8}$$

In this model, the term $U_{\mathrm{oc}}(\mathrm{SOC}(k))$ function is a nonlinear equation. The state and output equations in discrete time is expressed as follows:

$$\begin{aligned} x_{k+1} &= f(x_k, u_k) + w_k, \\ y_k &= g(x_k, u_k) + v_k, \end{aligned} \tag{9}$$

where $f(x_k, u_k)$ and $g(x_k, u_k)$ are continuously differentiable nonlinear functions, w_k is the process noise with zero means, and v_k is the measurement noise, which is independent of w_k with zero mean value.

The Strong Tracking Filter (STF) with online adaptively modified Kalman gain matrix and prior state error covariance to track the sudden change in the state vectors was used. The critical feature of the STF is the method to rearrange the prior error covariance $\mathbf{P}_k^-$ by multiplying it by a diagonal matrix $\mathbf{\Lambda}_k$ in which the differing diagonal entries optimize the propagation of components in state vector by diminishing the impacts of old data on current parameter estimation

$$\mathbf{P}_k^- = \mathbf{\Lambda}_k \mathbf{G}_k \mathbf{P}_{k-1}^+ \mathbf{G}_k + \beta_k \mathbf{Q}_k \beta_k, \tag{10}$$

where $\mathbf{\Lambda}_k$ denotes multiple fading factors matrix that is determined as

$$\mathbf{\Lambda}_k = \mathrm{diag}(\lambda_1, \lambda_1, \ldots, \lambda_n). \tag{11}$$

The proportion of λ and its constraint can be realized by prior knowledge of the system

$$\begin{aligned} \lambda_1 : \lambda_2 : \cdots : \lambda_n &= c_k(a_1 : a_2 : \cdots : a_n), \\ \lambda_i &= \max(1, c_k(a_i)), \end{aligned} \tag{12}$$

where $a_i \geq 1$, $i = 1, 2, \ldots, n$, are predetermined constants which reflect the distinctive fading rate of the state estimation, a_i is set to be of relatively larger value when it comes to circumstance that ith component in the state vector changes much faster as compared to the others, and c_k is the standard factor of λ_n that is given as follows:

$$\begin{aligned} V_k &= \begin{cases} S_1 S_1^T, & k = 0 \\ \dfrac{\rho V_{k-1} + S_k S_k^T}{1+\rho}, & k \geq 1, \end{cases} \\ N_k &= V_k - \beta R_k - H_k \beta_k Q_k \beta_k H_k^T, \\ M_k &= \mathrm{diag}(a_1, a_2, \ldots, a_n) G_k P_{k-1}^+ G_k^T H_k^T H_k, \\ c_k &= \frac{\mathrm{trace}(N_k)}{\mathrm{trace}(M_k)}, \end{aligned} \tag{13}$$

where S_k denotes the difference of output calculated by STF and measurement value. $\rho = 0.95$ and $\beta \geq 1$ are forgetting and weakening factors, respectively.

The STEKF was developed by applying the strong tracking algorithm on the EKF. STEKF benefits the estimation process by taking the advantages of EKF that minimizes the estimation error covariance and STF that track the state vector variation accurately. In addition, cubature Kalman filter generates a set of cubature points propagated by system equations to approximate the posterior estimate which was used. It can also track the fast-changing SOC value. As a result, the strong tracking with cubature on extended Kalman filter algorithm (STCEKF) was formed. For clarity, the steps in the algorithm of STCEKF are given as follows.

In the time update, the cubature points are generated

$$\begin{aligned} X_{i,k-1}^+ &= S_{k-1}^+ \varepsilon_i + \hat{x}_{k-1}^+, \quad i = 1, 2, \ldots, n, \\ \varepsilon_i &= \begin{cases} \sqrt{n}[1]_i, & i = 1, 2, \ldots, n \\ -\sqrt{n}[1]_i, & i = n+1, n+2, \ldots, 2n, \end{cases} \end{aligned} \tag{14}$$

where $S_{k-1}^+ (S_{k-1}^+)^T = P_{k-1}^+$ and n is the dimension of the state vector.

The cubature points are propagated

$$\overline{X}_{i,k} = g\left(X_{i,k-1}^+, u_{k-1}\right). \tag{15}$$

The predicted state is estimated

$$\hat{x}_k^- = \frac{1}{2n} \sum_{i=1}^{n} \overline{X}_{i,k}. \tag{16}$$

The predicted error covariance is calculated

$$P_k^- = \frac{1}{2n} \sum_{i=1}^{n} \overline{X}_{i,k} \left(\overline{X}_{i,k}\right)^T - x_k^- \left(x_k^-\right)^T + \beta_k Q_k \beta_k. \tag{17}$$

In the measurement update, the cubature points are generated

$$\widetilde{X}_{i,k} = S_k^- \varepsilon_i + \hat{x}_k^-, \quad i = 1, 2, \ldots, n. \tag{18}$$

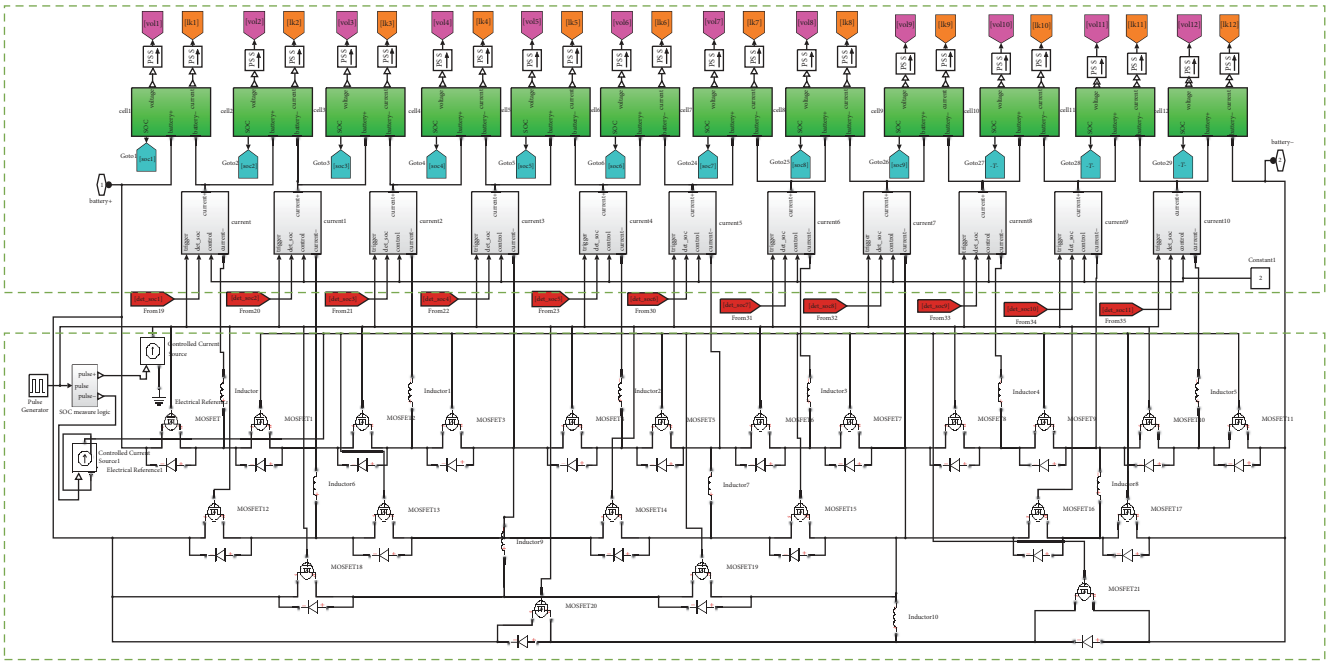

Figure 7: Example of battery model including SOC estimator (top) and cell balancing (bottom).

The propagated cubature points are evaluated

$$Z_{i,k} = h\left(\widetilde{X}_{i,k}, u_k\right). \tag{19}$$

The predicted measurement is estimated

$$\widehat{z}_k = \frac{1}{2n}\sum_{i=1}^{n} Z_{i,k}. \tag{20}$$

The innovation covariance matrix is obtained

$$P_{zz,k} = \frac{1}{2n}\sum_{i=1}^{n} Z_{i,k}\left(Z_{i,k}\right)^T - z_k\left(z_k\right)^T + \gamma_k R_k \gamma_k. \tag{21}$$

The cross-covariance matrix is determined

$$P_{xz,k} = \frac{1}{2n}\sum_{i=1}^{n} \widetilde{X}_{i,k}\left(Z_{i,k}\right)^T - \widehat{x}_k^-\left(\widehat{z}_k\right)^T. \tag{22}$$

The Kalman gain is calculated

$$K_k = P_{xz,k}\left(P_{zz,k}\right)^{-1}. \tag{23}$$

The updated state is estimated

$$x_k^+ = x_k^- + K_k\left(z_k - \widehat{z}_k\right). \tag{24}$$

The corresponding error covariance is computed

$$P_k^+ = P_k^- - K_k P_{zz,k}\left(K_k\right)^T. \tag{25}$$

The simulation model that includes the SOC estimation using STCEKF and the active cell balancing can be seen in Figure 7.

4. Experimental Tests

The battery was tested in a laboratory setup [8] as shown in Figure 8. The twelve lithium iron phosphate battery cells (ANR26650M1-B) were used during the test. The specifications of the cell can be obtained from a123batteries.com datasheet. The load current was generated by a DC electronic load while the battery cells were charged by a programmable DC power supply. It was used to control the voltage or current source with the output voltage (maximum at 36 V) and current (maximum at 20 A). The host PC communicates with the DAQ device to measure the charging and discharging of each cell. The NI DAQ device controlled the outputs and inputs data with acquisition rate set to 1 sample per second. A current sensor measured the current during the charging and discharge operation for one battery cell. As all the battery cells are unique due to the manufacturing variation, the test was repeated for other 11 cells. The experimental data for the 2-*RC* model for the 12 cells were obtained. The validated 2-*RC* models were updated into the series of lookup tables as shown in Figure 6.

4.1. Proposed Battery Model Validation. The prototype of the battery power system can be seen in Figure 9. The prototype was used to validate the 2-*RC* cell models at different ambient temperatures from 5°C, 15°C, 25°C, 35°C, and 45°C in an environmental chamber. For example, the root means square or RMS errors between the simulation and experimental results at 25°C for the 12-cell are shown in Table 2. The RMS error of Cell #1 terminal voltage between the simulation and experiment was around 7.20×10^{-5} at 25°C (see Table 2). The experimental data at a different ambient temperature of 25°C was compared with the model to test the robustness

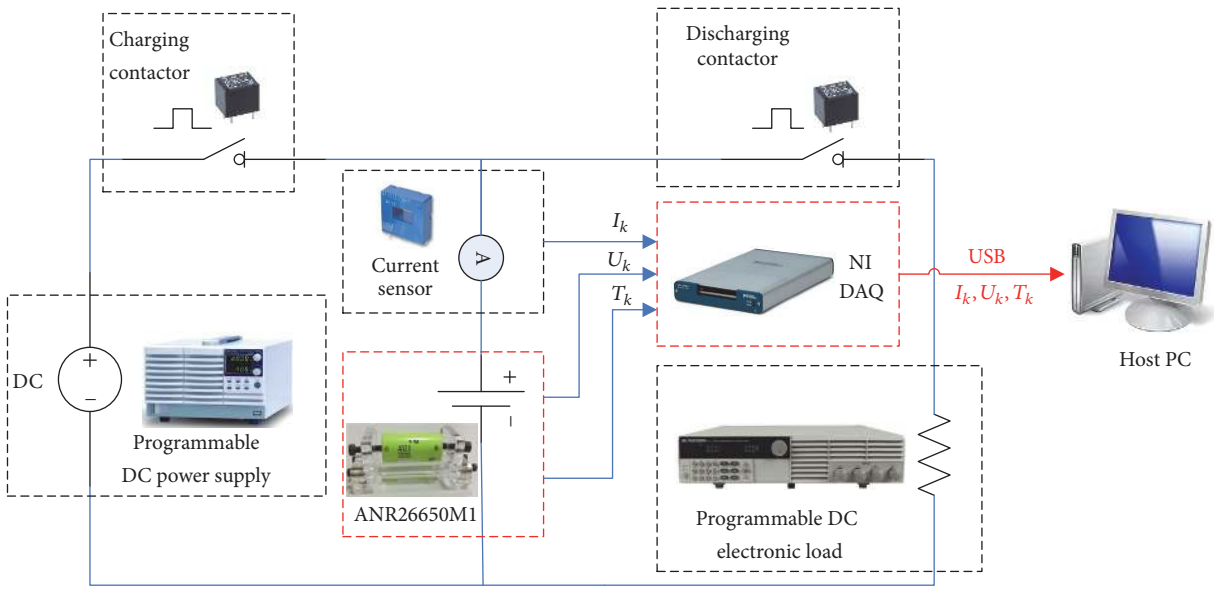

Figure 8: Test bench setup for battery cell testing [8].

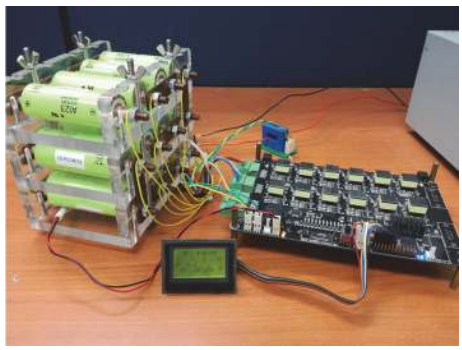

Figure 9: 12-cell battery pack prototype for multicell testing.

Table 2: RMSE between simulation and experiment of terminal voltage at 25°C.

Cell number	Root means square error (RMSE) of terminal voltage
Cell 01	2.26×10^{-05}
Cell 02	8.98×10^{-06}
Cell 03	1.88×10^{-05}
Cell 04	2.34×10^{-05}
Cell 05	2.54×10^{-05}
Cell 06	1.99×10^{-05}
Cell 07	2.37×10^{-05}
Cell 08	2.51×10^{-05}
Cell 09	1.92×10^{-05}
Cell 10	2.00×10^{-05}
Cell 11	1.74×10^{-05}
Cell 12	2.19×10^{-05}

of the numerical model in Figure 10. The result shows that the battery model output can estimate the terminal voltage with small error. The errors of the terminal voltage due to the current fluctuation can converge to zero within 1.20×10^{-5} s. The result showed that the proposed battery model was accurate. Note that the results are valid for the type of battery cells used.

4.2. SOC Estimation Algorithms Comparision. Several SOC estimation algorithms such as EKF, STEKF, CKF, STCEKF were compared using the 2-*RC* equivalent circuit battery cell models obtained at 25°C. The following test process was used to evaluate the proposed SOC estimation algorithm with other algorithms.

(1) Initialization. To determine the benchmark of the SOC, the battery cell needs to be fully charged followed by a 15-hour relaxation period before running the algorithms. It helped to ensure that the initial SOC of the battery cell is 100% in its equilibrium state.

(2) Compute Actual SOC. A reference ampere-hour method was used to determine the actual SOC for comparison.

(3) Test Different Algorithms. An initial SOC error was set to 20% for testing the convergence performance using different SOC estimation algorithms.

(4) Comparison Process. The root means square error (RMSE) was computed to evaluate the estimation performance for various SOC estimation algorithms. As shown in Figure 11, the initial transient stage of the SOC estimation was quite

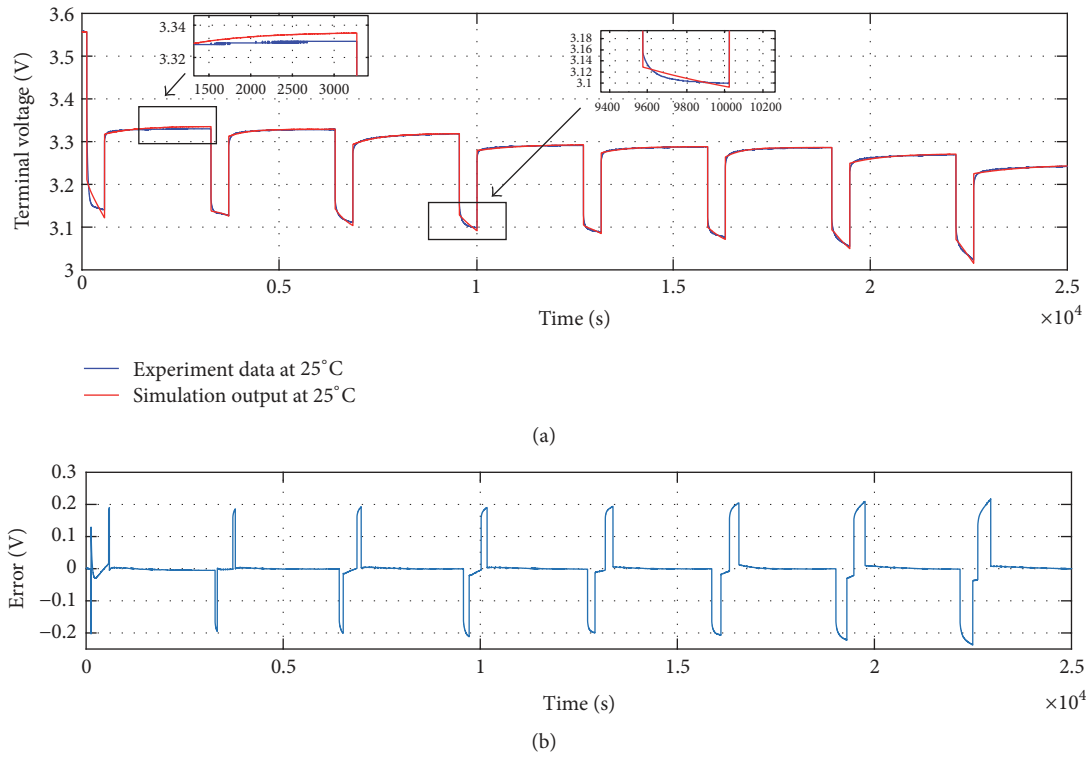

Figure 10: (a) Cell #1 model validated at 25°C. (b) Cell #1 error between simulation and experiment results at 25°C.

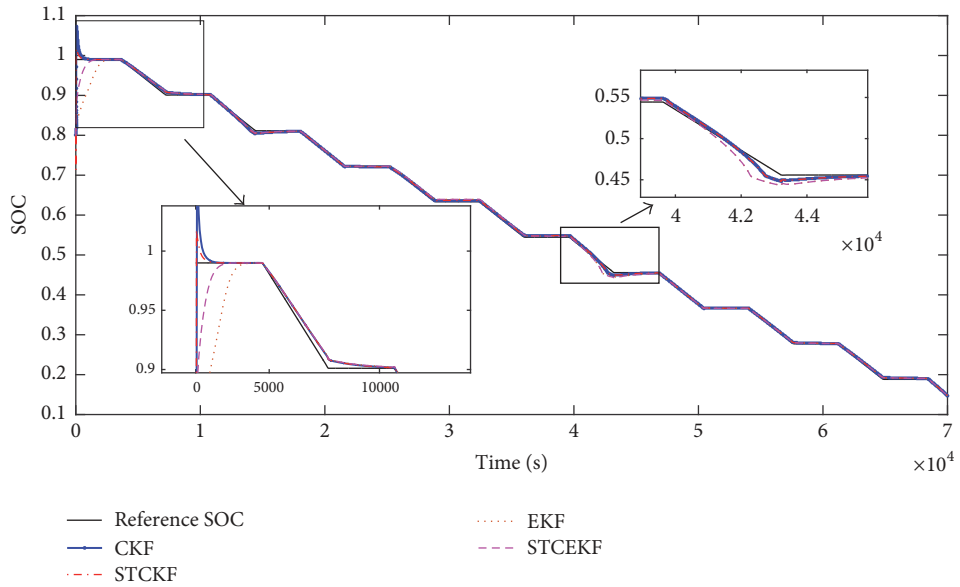

Figure 11: SOC estimation results using EKF, STEKF, CKF, and STCEKF at 25°C.

different for each method. The CKF exhibits an overshoot while EKF was quite sluggish in the response. As compared to the STCEKF, there was a smaller overshoot with a faster response as compared to the other methods. However, the STEKF deviated from the reference SOC curve during the discharging. Most of the SOC estimation results could converge to the reference SOC. The RMSE values and the convergence time of the SOC estimation are tabulated in Table 3. It can be seen that STCEKF exhibits the smallest RMSE and the shorter convergence time as compared to other methods. Therefore, the STCEKF has faster and more accurate SOC estimation as compared to EKF, STEKF, and CKF. Note that similar behavior can be found at a different temperature.

Table 3: RMSE for SOC estimation using EKF, STEKF, CKF, and STCEKF at 25°C.

Descriptions	Extended Kalman filter (EKF)	Strong tracking extended Kalman filter (STEKF)	Cubature Kalman filter (CKF)	Strong tracking with cubature on extended Kalman filter (STCEKF)
Root means square error (RMSE)	0.02735	0.01455	0.01223	0.01176
Convergence time (min)	35	20	11.7	10

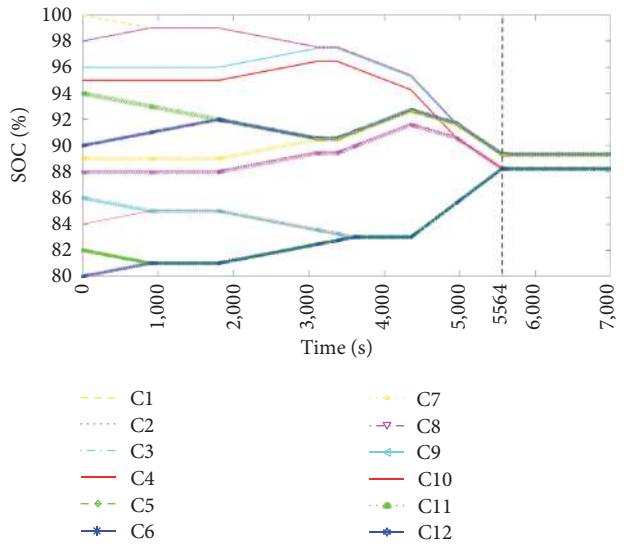

Figure 12: Active cell balancing results using proposed active cell balancing circuit for all cells at 25°C.

As mentioned in the above section, the balancing routine was used to balance the imbalanced cells. Firstly, the balancing routine will seek for the lowest, highest, and average SOC of the cells. The cell number with the lowest and highest SOC will be logged. Secondly, the balancing routine will determine whether the BMS has been balanced by using the lowest, highest, and average SOC of the cells. If all the cells were balanced, the balancing routine would turn off all the relays that control the active cell balancing. Thirdly, the balancing routine will execute the balancing for the cell with the lowest SOC first. Note that one DC-DC converter will be used to balance Cell #1 to #6, and another DC-DC converter will be used to balance Cell #7 to #12.

Figure 12 shows the experimental results of SOC for each cell (labeled as C1 to C12) after the active cell balancing. As seen in Figure 12, the SOC of each cell was maintained at the same value at the end of the cell balancing. Most of the cells exhibited same SOC value at the end of the balancing time frame of 5564 s. The SOC of each cell converged to similar value while the battery pack was running. It did not have to wait for 5564 s for powering. A comparative study between different active balancing topologies was shown in Table 4 to further examine the balancing speed and the balancing loss between these methods. In Table 4, the capacitors showed a slower balancing speed than the transformer. Although the proposed algorithm for the active cell balancing method was slightly complicated than other methods, it demonstrated some merits of higher balancing speed and lower balancing loss for the battery management system. For brevity, only the cell balancing test at 25°C was shown. The similar test at different ambient temperatures can be repeated.

4.3. SOC Estimation under Realistic Load Profile and Varying Ambient Temperature. To further validate the proposed ambient temperature model and SOC estimation algorithm under the practical and dynamic situation, the New European Driving Cycle load profile [49] was applied to the 12-cell series battery pack prototype to simulate the electric vehicle applications under varying the ambient temperature. The ambient temperature variation can be seen in Figure 13(a). The current load profile of the electric vehicle subjected to the temperature disturbance is depicted in Figure 13(b). The load profile was scaled down to fit the battery pack. However, it can be adjusted to different current level. The programmable DC electronic load was used to run the preprogrammed load profile. Before the experiment, the battery pack was fully charged to 100% in Figure 13(c). The instantaneous error was determined based on the difference between the respective methods (i.e., STCEKF and EKF) and the actual SOC value obtained by the Ah counting method. As observed in Figure 13(c), the proposed SOC estimation can follow the actual SOC value by the Ah counting method under the changing operating ambient temperature. Despite the ambient temperature perturbation, the SOC error of the STCEKF method (see Figure 13(d)) settled to a smaller steady-state error after a short period of drift as compared to EKF-based SOC model that was unable to recover from the ambient temperature disturbances. In summary, the proposed STCEKF is more robust than EKF in the SOC estimation. The graphs for the STEKF and CKF were not available at the time of comparison. In addition, the tests can be repeated for different cell type and current load profiles at different temperatures.

5. Conclusions

The first strong tracking cubature extended Kalman filter (STCEKF) and active cell balancing for the lithium iron phosphate battery system model were jointly developed. The SOC estimation using the STCEKF produced the lowest error and faster computational time as compared with the extended Kalman filter (EKF). A new cell balancing circuit and algorithm showed a higher balancing speed and less balancing loss during the charging and discharging. The proposed battery power system design was validated by both model simulation and experiment using the actual battery prototype. The New European Driving Cycle load profile

Table 4: Comparison of different active cell balancing methods at 25°C.

	Capacitor	Switched capacitor (STSC)	Inductor	Proposed method	Transformer
Balancing speed	11330 s	8550 s	6833 s	5564 s	6064 s
Average state-of-charge (efficiency)	90.0%	90.0%	89.2%	89.5%	89.3%
Cost	4	3	3	3	1
Size	3	2	3	3	1
Complexity	4	4	1	2	3

Note. Cost (4: cheap, 1: expensive); size (4: small, 1: big); complexity (4: low, 1: high).

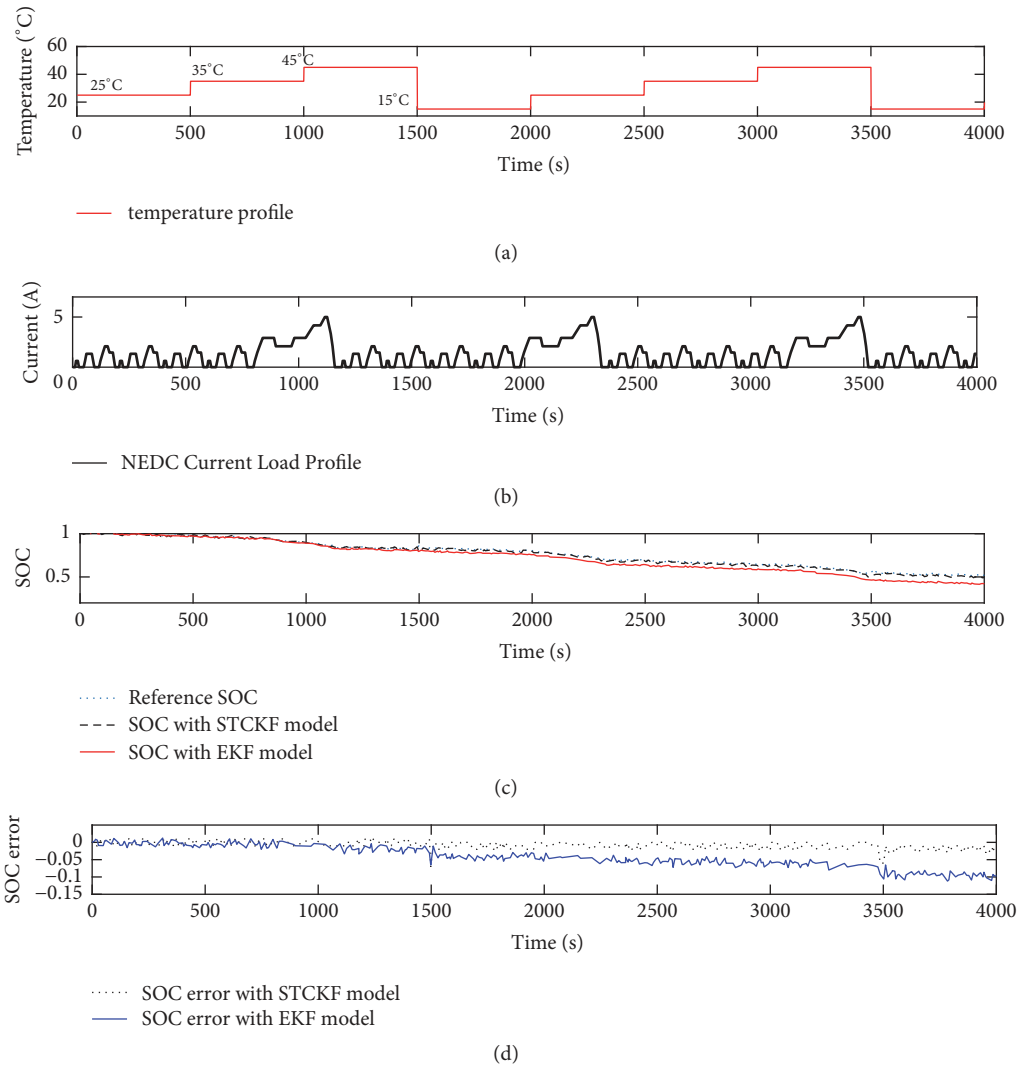

Figure 13: (a) Ambient temperature profile; (b) current profile; (c) SOC comparison of proposed STCKF and EKF-based model; (d) SOC error comparison.

for an electric vehicle was used to verify and compare the proposed SOC estimation performance by the STCEKF with the EKF. The experimental results showed that the STCEKF performed better than the EKF under the varying ambient temperature and current load profile (that was equivalent to the actual load profile in the electric vehicle). In summary, the proposed STCEKF was successfully implemented and validated in the actual 12-cell battery pack with less SOC estimation error, faster balancing time, and less balancing loss for real-time application. For future works, the battery

model will be fine-tuned and further developed to detect and diagnose uncertain faults subjected to external disturbances with less computation burden.

Conflicts of Interest

The authors declare that there are no conflicts of interest regarding the publication of this paper.

Acknowledgments

The authors would like to acknowledge Newcastle University in Singapore and Temasek Polytechnic for providing the necessary financial support and equipment.

References

[1] P. Germano and Y. Perriard, "Battery Charger for Electric Vehicle Based on a Wireless Power Transmission," in *Proceedings of the 13th IEEE Vehicle Power and Propulsion Conference, VPPC 2016*, China, October 2016.

[2] O. Gomozov, J. P. Trovao, X. Kestelyn, and M. R. Dubois, "Adaptive Energy Management System Based on a Real-Time Model Predictive Control With Nonuniform Sampling Time for Multiple Energy Storage Electric Vehicle," *IEEE Transactions on Vehicular Technology*, vol. 66, no. 7, pp. 5520–5530, 2017.

[3] E. A. Grunditz and T. Thiringer, "Performance Analysis of Current BEVs Based on a Comprehensive Review of Specifications," *IEEE Transactions on Transportation Electrification*, vol. 2, no. 3, pp. 270–289, 2016.

[4] H. Cave, "Charging ahead? the bid for better batteries," *Journal of Engineering and Technology*, vol. 12, no. 2, pp. 58–61, 2017.

[5] A. Castaings, W. Lhomme, R. Trigui, and A. Bouscayrol, "Practical control schemes of a battery/supercapacitor system for electric vehicle," *IET Electrical Systems in Transportation*, vol. 6, no. 1, pp. 20–26, 2016.

[6] Y. Wang, H. Fang, Z. Sahinoglu, T. Wada, and S. Hara, "Adaptive Estimation of the State of Charge for Lithium-Ion Batteries: Nonlinear Geometric Observer Approach," *IEEE Transactions on Control Systems Technology*, vol. 23, no. 3, pp. 948–962, 2015.

[7] Y. Xing, W. He, M. Pecht, and K. L. Tsui, "State of charge estimation of lithium-ion batteries using the open-circuit voltage at various ambient temperatures," *Applied Energy*, vol. 113, pp. 106–115, 2014.

[8] Z. Gao, C. S. Chin, W. L. Woo, and J. Jia, "Integrated equivalent circuit and thermal model for simulation of temperature-dependent LiFePO4 battery in actual embedded application," *Energies*, vol. 10, no. 1, article 85, 2017.

[9] T. K. Dong, A. Kirchev, F. Mattera, J. Kowal, and Y. Bultel, "Dynamic modeling of Li-ion batteries using an equivalent electrical circuit," *Journal of The Electrochemical Society*, vol. 158, no. 3, pp. A326–A336, 2011.

[10] D. Andre, M. Meiler, K. Steiner, H. Walz, T. Soczka-Guth, and D. U. Sauer, "Characterization of high-power lithium-ion batteries by electrochemical impedance spectroscopy. II: Modelling," *Journal of Power Sources*, vol. 196, no. 12, pp. 5349–5356, 2011.

[11] X. S. Hu, S. B. Li, and H. Peng, "A comparative study of equivalent circuit models for Li-ion batteries," *Journal of Power Sources*, vol. 198, pp. 359–367, 2012.

[12] W. Waag, C. Fleischer, and D. U. Sauer, "Critical review of the methods for monitoring of lithium-ion batteries in electric and hybrid vehicles," *Journal of Power Sources*, vol. 258, pp. 321–339, 2014.

[13] S. G. Li, S. M. Sharkh, F. C. Walsh, and C. N. Zhang, "Energy and battery management of a plug-in series hybrid electric vehicle using fuzzy logic," *IEEE Transactions on Vehicular Technology*, vol. 60, no. 8, pp. 3571–3585, 2011.

[14] W. He, N. Williard, C. Chen, and M. Pecht, "State of charge estimation for Li-ion batteries using neural network modeling and unscented Kalman filter-based error cancellation," *International Journal of Electrical Power & Energy Systems*, vol. 62, pp. 783–791, 2014.

[15] S.-C. Wang and Y.-H. Liu, "A PSO-Based Fuzzy-Controlled Searching for the Optimal Charge Pattern of Li-Ion Batteries," *IEEE Transactions on Industrial Electronics*, vol. 62, no. 5, pp. 2983–2993, 2015.

[16] P. Melin and O. Castillo, "Intelligent control of complex electrochemical systems with a neuro-fuzzy-genetic approach," *IEEE Transactions on Industrial Electronics*, vol. 48, no. 5, pp. 951–955, 2001.

[17] H. Chen and G. Wu, "Compensation fuzzy neural network power management strategy for hybrid electric vehicle," *Tongji Daxue Xuebao/Journal of Tongji University*, vol. 37, no. 4, pp. 525–530, 2009.

[18] V. Klass, M. Behm, and G. Lindbergh, "Capturing lithium-ion battery dynamics with support vector machine-based battery model," *Journal of Power Sources*, vol. 298, pp. 92–101, 2015.

[19] P. Gao, C. Zhang, and G. Wen, "Equivalent circuit model analysis on electrochemical impedance spectroscopy of lithium metal batteries," *Journal of Power Sources*, vol. 294, pp. 67–74, 2015.

[20] J. Smekens, J. Paulsen, W. Yang et al., "A Modified Multiphysics model for Lithium-Ion batteries with a $Li_xNi_{1/3}Mn_{1/3}Co_{1/3}O_2$ electrode," *Electrochimica Acta*, vol. 174, Article ID 25140, pp. 615–624, 2015.

[21] H. Fang, Y. Wang, Z. Sahinoglu, T. Wada, and S. Hara, "State of charge estimation for lithium-ion batteries: An adaptive approach," *Control Engineering Practice*, vol. 25, no. 1, pp. 45–54, 2014.

[22] J. Du, Z. Liu, and Y. Wang, "State of charge estimation for Li-ion battery based on model from extreme learning machine," *Control Engineering Practice*, vol. 26, no. 1, pp. 11–19, 2014.

[23] J. Du, Z. Liu, C. Chen, and Y. Wang, "Li-ion battery SOC estimation using EKF based on a model proposed by extreme learning machine," in *Proceedings of the 7th IEEE Conference on Industrial Electronics and Applications*, pp. 1648–1653, Singapore, Singapore, 2012.

[24] A. Densmore and M. Hanif, "Modeling the condition of lithium ion batteries using the extreme learning machine," in *Proceedings of the 2016 IEEE PES PowerAfrica Conference, PowerAfrica 2016*, pp. 184–188, Livingstone, Zambia, July 2016.

[25] R. Razavi-Far, S. Chakrabarti, and M. Saif, "Multi-step parallel-strategy for estimating the remaining useful life of batteries," in *Proceedings of the 2017 IEEE 30th Canadian Conference on Electrical and Computer Engineering (CCECE)*, pp. 1–4, Windsor, ON, Canada, April 2017.

[26] M. Doyle, T. Fuller, and J. Newman, "Modeling of galvanostatic charge and discharge of the lithium/ polymer/insertion cell," *Journal of The Electrochemical Society*, vol. 140, no. 6, pp. 1526–1533, 1993.

[27] T. F. Fuller, M. Doyle, and J. Newman, "Simulation and optimization of the dual lithium ion insertion cell," *Journal of The Electrochemical Society*, vol. 141, no. 1, pp. 1–10, 1994.

[28] S. Atlung, K. West, and T. Jacobsen, "Dynamic Aspects of Solid Solution Cathodes for Electrochemical Power Sources," *Journal of The Electrochemical Society*, vol. 126, no. 8, pp. 1311–1321, 1979.

[29] S. Khaleghi Rahimian, S. Rayman, and R. E. White, "Extension of physics-based single particle model for higher charge-discharge rates," *Journal of Power Sources*, vol. 224, pp. 180–194, 2013.

[30] K. A. Smith, C. D. Rahn, and C.-Y. Wang, "Model-based electrochemical estimation of lithium-ion batteries," in *Proceedings of the 17th IEEE International Conference on Control Applications, CCA*, pp. 714–719, USA, September 2008.

[31] G. L. Plett, "Extended Kalman filtering for battery management systems of LiPB-based HEV battery packs—part 1. Background," *Journal of Power Sources*, vol. 134, no. 2, pp. 252–261, 2004.

[32] G. L. Plett, "Extended Kalman filtering for battery management systems of LiPB-based HEV battery packs—part 2. Modeling and identification," *Journal of Power Sources*, vol. 134, no. 2, pp. 262–276, 2004.

[33] G. L. Plett, "Extended Kalman filtering for battery management systems of LiPB-based HEV battery packs: part 3. State and parameter estimation," *Journal of Power Sources*, vol. 134, no. 2, pp. 277–292, 2004.

[34] X. Chen, W. Shen, Z. Cao, and A. Kapoor, "A novel approach for state of charge estimation based on adaptive switching gain sliding mode observer in electric vehicles," *Journal of Power Sources*, vol. 246, pp. 667–678, 2014.

[35] D. Kim, K. H. Koo, J. J. Jeong, T. D. Goh, and S. W. Kim, "Second-order discrete-time sliding mode observer for state of charge determination based on a dynamic resistance Li-ion battery model," *Energies*, vol. 6, no. 10, pp. 5538–5551, 2013.

[36] X. Hu, F. Sun, and Y. Zou, "Estimation of state of charge of a Lithium-Ion battery pack for electric vehicles using an adaptive luenberger observer," *Energies*, vol. 3, no. 9, pp. 1586–1603, 2010.

[37] T. He, D. Li, Z. Wu, Y. Xue, and Y. Yang, "A modified luenberger observer for SOC estimation of lithium-ion battery," in *Proceedings of the 2017 36th Chinese Control Conference (CCC)*, pp. 924–928, Dalian, China, July 2017.

[38] Y. Wang, H. Fang, L. Zhou, and T. Wada, "Revisiting the State-of-Charge Estimation for Lithium-Ion Batteries: A Methodical Investigation of the Extended Kalman Filter Approach," *IEEE Control Systems Magazine*, vol. 37, no. 4, pp. 73–96, 2017.

[39] S. Santhanagopalan and R. E. White, "State of charge estimation using an unscented filter for high power lithium ion cells," *International Journal of Energy Research*, vol. 34, no. 2, pp. 152–163, 2010.

[40] R. Klein, N. A. Chaturvedi, J. Christensen, J. Ahmed, R. Findeisen, and A. Kojic, "Electrochemical model based observer design for a lithium-ion battery," *IEEE Transactions on Control Systems Technology*, vol. 21, no. 2, pp. 289–301, 2013.

[41] I. Arasaratnam and S. Haykin, "Cubature Kalman filters," *Institute of Electrical and Electronics Engineers Transactions on Automatic Control*, vol. 54, no. 6, pp. 1254–1269, 2009.

[42] J. Jia, P. Lin, C. S. Chin et al., "Multirate strong tracking extended Kalman filter and its implementation on lithium iron phosphate (LiFePO4) battery system," in *Proceedings of the 11th IEEE International Conference on Power Electronics and Drive Systems, PEDS 2015*, pp. 640–645, Australia, June 2015.

[43] P. Malysz, R. Gu, J. Ye, H. Yang, and A. Emadi, "State-of-charge and state-of-health estimation with state constraints and current sensor bias correction for electrified powertrain vehicle batteries," *IET Electrical Systems in Transportation*, vol. 6, no. 2, pp. 136–144, 2016.

[44] Z. Chen, S. Qiu, M. A. Masrur, and Y. L. Murphey, "Battery state of charge estimation based on a combined model of extended kalman filter and neural networks," in *Proceedings of the 2011 International Joint Conference on Neural Network, IJCNN 2011*, pp. 2156–2163, USA, August 2011.

[45] A. Sidhu, A. Izadian, and S. Anwar, "Adaptive nonlinear model-based fault diagnosis of li-ion batteries," *IEEE Transactions on Industrial Electronics*, vol. 62, no. 2, pp. 1002–1011, 2015.

[46] X. He, Z. Wang, X. Wang, and D. H. Zhou, "Networked strong tracking filtering with multiple packet dropouts: algorithms and applications," *IEEE Transactions on Industrial Electronics*, vol. 61, no. 3, pp. 1454–1463, 2014.

[47] T. Kim, W. Qiao, and L. Qu, "Power electronics-enabled self-X multicell batteries: A design toward smart batteries," *IEEE Transactions on Power Electronics*, vol. 27, no. 11, pp. 4723–4733, 2012.

[48] M. Daowd, N. Omar, P. van den Bossche, and J. van Mierlo, "A review of passive and active battery balancing based on MATLAB/Simulink," *International Review of Electrical Engineering*, vol. 6, no. 7, pp. 2974–2989, 2011.

[49] Z. Gao, C. Chin, J. Chiew, J. Jia, and C. Zhang, "Design and Implementation of a Smart Lithium-Ion Battery System with Real-Time Fault Diagnosis Capability for Electric Vehicles," *Energies*, vol. 10, no. 10, p. 1503, 2017.

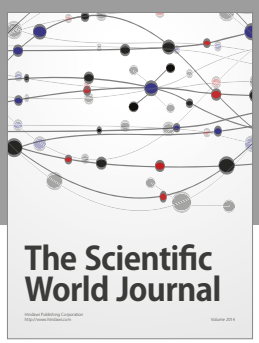

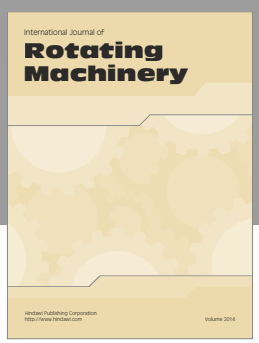

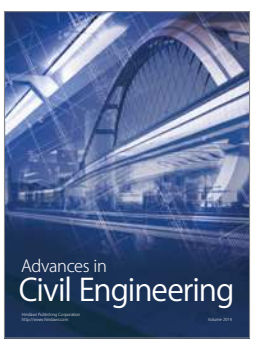

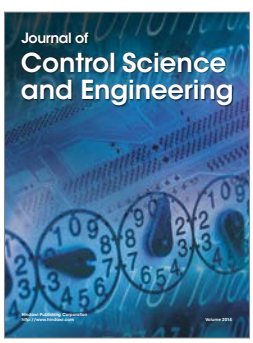

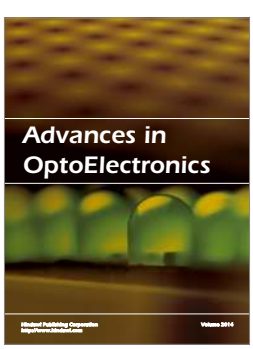

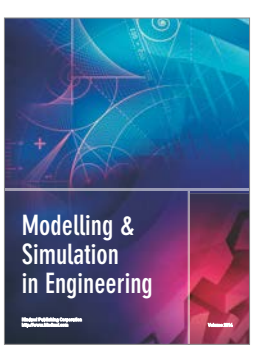

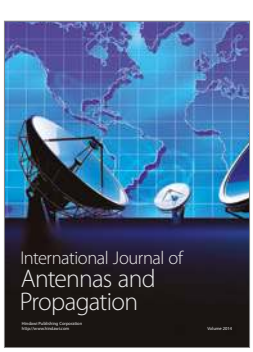

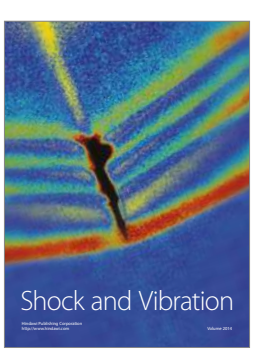

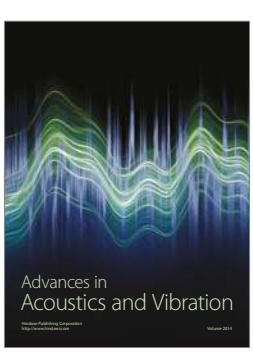

Hindawi

Submit your manuscripts at
https://www.hindawi.com